PAPER

NJC
www.rsc.org/njc

Microwave approach for the synthesis of rhabdophane-type lanthanide orthophosphate (Ln = La, Ce, Nd, Sm, Eu, Gd and Tb) nanorods under solvothermal conditions†

Chitta Ranjan Patra, Gabashvili Alexandra, Sujata Patra, David Solomon Jacob, Aharon Gedanken,* Asher Landau and Yossi Gofer

Department of Chemistry and Kanbar Laboratory for Nanomaterials, Bar-Ilan University Center for Advanced Materials and Nanotechnology, Bar-Ilan University, Ramat-Gan, 52900, Israel. E-mail: gedanken@mail.biu.ac.il; Fax: +972-3-535-1250; Tel: +972-3-531-8315

Received (in Montpellier, France) 10th October 2004, Accepted 27th January 2005
First published as an Advance Article on the web 1st April 2005

Rhabdophane-type hexagonal lanthanide orthophosphate, $LnPO_4 \cdot nH_2O$ (Ln = La, Ce, Nd, Sm, Eu, Gd and Tb, n = 0 to 0.6), and body-centered tetragonal $ErPO_4 \cdot nH_2O$ nanowires/nanorods have been successfully synthesized in high yield (>95%) by simple microwave heating of an aqueous solution of Ln(III) nitrate and $NH_4H_2PO_4$ in the pH range 1.8–2.2. The reaction was conducted in a simple domestic microwave oven. The structure, morphology, composition and physical properties of the as-prepared products have been characterized by powder X-ray diffraction, low resolution transmission electron microscopy, high resolution transmission electron microscopy, selected area electron diffraction, thermogravimetric analysis, differential scanning calorimetry, infrared spectroscopy, Raman spectroscopy, X-ray photoelectron spectroscopy, and photoluminescence spectroscopy. The length and width of the resulting lanthanide orthophosphate nanowires/nanorods are in the range 70–2200 nm and 6–130 nm, respectively. A possible mechanism for the formation of $LnPO_4 \cdot nH_2O$ nanowires/nanorods is briefly discussed.

Introduction

Recently, numerous methods for the synthesis of nanoparticles, nanotubes, nanowires, and nanorods with desired particle sizes and controlled morphology have been developed.[1] These nanomaterials with different shapes have recently gained interest and importance based on their novel properties associated with their reduced dimensionality and their potential applications in nanotechnologies.[1,2–5] Among the large number of lanthanide salts[6,7] (oxides, borates and fluorides), lanthanide orthophosphate ($LnPO_4$) nanomaterials are the most important from academic as well as industrial points-of-view due to their unique properties. Rare earth orthophosphates ($LnPO_4$) possess a variety of potentially beneficial properties such as very high thermal stability (~2300 °C),[8] low solubility (K_{sp} = 10^{-25} to 10^{-27}) in water,[9] a high refractive index ($n \approx 1.5$) and a high concentration of lasing ions (~1.8×10^{21} ions cm^{-3}).[10] Because of these unique properties, $LnPO_4$ can be used in various applications, such as luminescent or laser materials,[2,11,12] magnets,[13] ceramics,[8] catalysts,[14] proton conductors, moisture sensors, heat-resistant materials, hosts for radioactive nuclear waste,[11,12,15] green ($^5D_4$–$^7F_5$ of Tb^{3+} at 543 nm) phosphor (for Tb^{3+} co-activated by bulk $LaPO_4$) in fluorescent lamps,[11,12] scintillators for X-ray and γ-ray detection in medical science, biochemical probes and medical diagnostics.[16]

Because of the growing importance of $LnPO_4$, several authors have reported the synthesis of these materials *via* various methods. However, the reported conventional methods for the synthesis of $LnPO_4$ nanomaterials take long times (12 h) or require high temperatures, high pressures, expensive precursors, or specific complexing agents. There exists one microwave technique[17] for the synthesis of $LnPO_4$, but it is a solid state reaction that requires P_2O_5, a highly toxic and corrosive material. These problems are limiting factors in the development of $LnPO_4$ nanorods. The aim of our present work was to establish an efficient, fast and simple solvothermal method that avoids the above-mentioned drawbacks for the synthesis of $LnPO_4$. In the present article, we report a new technique for the synthesis of rhabdophane-type[18,19] hexagonal $LnPO_4 \cdot nH_2O$ (Ln = La, Ce, Nd, Sm, Eu, Gd and Tb) nanorods using microwave-assisted solvothermal synthesis in a simple domestic microwave oven (DMO). To the best of our knowledge, this method has never been used before for the synthesis of $LnPO_4 \cdot nH_2O$ nanorods.

Experimental

Microwave–assisted synthesis of lanthanide orthophosphate hydrates

All lanthanide(III) nitrates and $NH_4H_2PO_4$ with >99.9% purity were purchased from Aldrich Co. and used as received without further purification. $LnPO_4 \cdot nH_2O$ nanomaterials were prepared by microwave heating of an aqueous solution of Ln(III) nitrate and $NH_4H_2PO_4$ at atmospheric pressure in an open system. The microwave refluxing apparatus was a modified domestic microwave oven (900 W with a frequency of 2.45 GHz), described elsewhere.[20]

In a typical synthesis, 20 ml of aqueous 0.05 M $NH_4H_2PO_4$ were added to 20 ml of a 0.05 M aqueous solution of $Ln(NO_3)_3$ (Ln = La, Ce, Nd, Sm, Eu, Gd, Tb and Er) in a 100 ml round-bottomed flask. A colloidal precipitate, without any special morphology, was obtained upon the addition of $NH_4H_2PO_4$ to

† Electronic supplementary information (ESI) available: HRTEM analysis micrographs of as-synthesized $LnPO_4 \cdot nH_2O$ (Ln = Ce, Sm and Tb); FTIR and Raman spectra of as-synthesized hexagonal $LnPO_4 \cdot nH_2O$ (Ln = La, Ce, Nd, Sm, Eu, Gd, Tb) and tetragonal $ErPO_4 \cdot nH_2O$; XPS spectra of as-synthesized $CePO_4 \cdot nH_2$ and $NdPO_4 \cdot nH_2O$. See http://www.rsc.org/suppdata/nj/b4/b415693e/

DOI: 10.1039/b415693e

Table 1 Experimental conditions, yield, BET surface area, XRD and TEM data of rhabdophane-type $LnPO_4 \cdot nH_2O$ synthesized from $Ln(NO_3)_3$ and $NH_4H_2PO_4$ under microwave irradiation.

					XRD		TEM	
Entry	$Ln(NO_3)_3$	Lanthanide orthophosphate $LnPO_4 \cdot nH_2O$[a]	Yield/wt %	BET surface area/$m^2\ g^{-1}$	JCPDS No.	Length/nm	Width/nm	Morphology
1	$La(NO_3)_3$	$LaPO_4 \cdot 0.5H_2O$	98.3	127	46–1439	70–180	6–9	Nanorods
2	$Ce(NO_3)_3$	$CePO_4 \cdot H_2O$	99.1	114	35–0614	130–240	8–9	Nanorods
3	$Nd(NO_3)_3$	$NdPO_4 \cdot 0.5H_2O$	95.3	110	34–0535	210–350	7–9	Nanorods
4	$Sm(NO_3)_3$	$SmPO_4 \cdot 0.5H_2O$	99.8	112	34–0537	70–790	8–9	Nanorods
5	$Eu(NO_3)_3$	$EuPO_4 \cdot H_2O$	97.3	105	20–1044	70–180	6–9	Nanorods
6	$Gd(NO_3)_3$	$GdPO_4 \cdot H_2O$	99.3	110	39–0232	100–300	6–7	Nanorods
7	$Tb(NO_3)_3$	$TbPO_4 \cdot H_2O$	98.4	86	20–1244	$1.1–2.2 \times 10^3$ $0.5–1.5 \times 10^3$	80–130 6–8	Nanorods Nanowires
8	$Er(NO_3)_3$	$ErPO_4 \cdot 0.3H_2O$	98.2	90	20–0391	20–100	N/A	Nanoparticles

[a] According to EDX analysis giving Ln/P/O atomic ratio of ~1 : 1 : 4 to 1 : 1 : 4.5. All as-prepared samples were highly crystalline as confirmed by XRD.

the $Ln(NO_3)_3$ solution. The pH of the solution before and after the reaction was in the range of 1.8–2.2. The sample was irradiated for 20 min with 60% of the instrument's power (on/off irradiation cycles ratio of 3/2) in order to control the reaction and reduce the risk of overheating the solvent in open air atmosphere (except for $CePO_4 \cdot nH_2O$, which was carried out under argon to prevent the oxidation of Ce^{3+} to Ce^{4+}). The resulting products were collected, centrifuged at 9000 rpm, washed several times using ethanol and distilled water, and then dried overnight under vacuum at room temperature. Yields and selected data of the as-prepared products (>95%) are listed in Table 1. The above experiments were conducted several times and showed good reproducibility.

Characterization techniques

The structure and phase purity of the as-synthesized samples were determined by X-ray diffraction (XRD) analysis using a Bruker AXS D8 Advance Powder X-ray diffractometer (using CuKα radiation: λ = 1.5418 Å). The surface areas were measured by N_2 adsorption and calculated using the BET multipoint equation with a Micrometrics Gemini instrument. Particle morphologies (microstructures of the samples) was studied by low resolution transmission electron microscopy (LRTEM) on a Jeol-JEM 100SX microscope, working at a 100 kV accelerating voltage. High resolution transmission electron microscopy (HRTEM) micrographs were taken using a Jeol 2010 with 200 kV accelerating voltage. TGA of the as-synthesized samples were carried out under a stream of nitrogen at a heating rate of 10 °C min^{-1} from 25 °C to 600 °C using a Mettler Toledo TGA/STDA 851. DSC analysis, from 20 °C to 600 °C, of the as-synthesized samples was carried out on Mettler Toledo TC15, using a stream of nitrogen (20 ml min^{-1}) at a heating rate of 4 °C min^{-1} in a crimped aluminium crucible. Fourier transform infrared spectroscopy (FTIR) analysis was measured with a Coulter (Nicolet Impact-410) infrared spectrometer on KBr pellets in the region of 400–4000 cm^{-1} with a 4 cm^{-1} resolution under ambient conditions. A Raman Division Instrument (Jobin Yvon Horiba) was used with the λ = 514.5 nm line of an Ar laser as the excitation source at ambient temperature. The X-ray photoelectron spectroscopy (XPS) spectra were accumulated on an AXIS HS (Kratos Analytical) electron spectrometer system with a monochromated Al K standard X-ray source. The excitation and emission (fluorescence) spectra were recorded on an Aminco-Bowman-Series-2 Luminescence spectrophotometer equipped with a 150 W xenon lamp as the excitation source.

Results and discussion

X-Ray diffraction studies

The crystal structures of the as-synthesized lanthanide orthophosphate products $LnPO_4 \cdot nH_2O$ (Ln = La, Ce, Nd, Sm, Eu, Gd, Tb and Er) were identified by X-ray diffraction analysis (Fig. 1). The XRD patterns indicate that the products are crystalline. All reflections can be distinctly indexed to a rhabdophane-type pure hexagonal phase for Ln = La, Ce, Nd, Sm, Eu, Gd and Tb and a body-centered tetragonal (bct) structure for Ln = Er. It can also be observed in Fig. 1 that XRD analyses show systematic shifts in the position of the diffraction peaks, reflecting the contraction of the ionic radii of the lanthanides. The different phase observed for $ErPO_4 \cdot nH_2O$ might be due to lanthanide contraction. The diffraction peaks are consistent with standard data files (see JCPDS card numbers in Table 1). However, XRD patterns of Tb, Gd and La phosphates show an impurity at low angle (11–12°).

BET measurements

The BET surface area of the as-synthesized$LnPO_4 \cdot nH_2O$ are found to be in the range 86–127 $m^2\ g^{-1}$ (Table 1). The high specific surface areas of these particles are due to their nanocrystalline nature. The lower values observed for $TbPO_4 \cdot nH_2O$ nanorods and $ErPO_4 \cdot nH_2O$ nanoparticles may be due to the larger size of the former [see Fig. 2(g) below] and the aggregated nature of the latter [see Fig. 2(h) below].

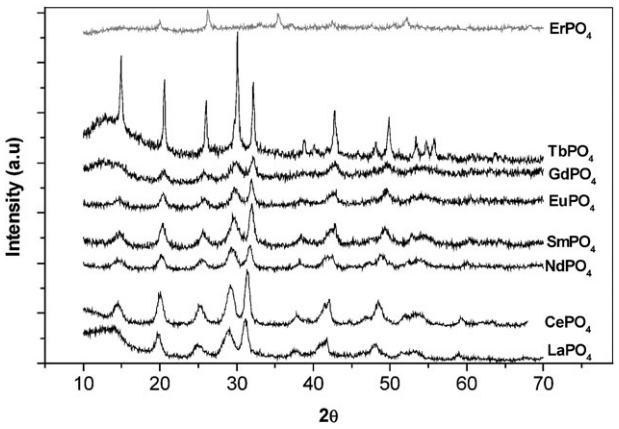

Fig. 1 XRD patterns of as-synthesized $LnPO_4 \cdot nH_2O$ (Ln = La, Ce, Nd, Sm, Eu, Gd, Tb, Er) nanostructures.

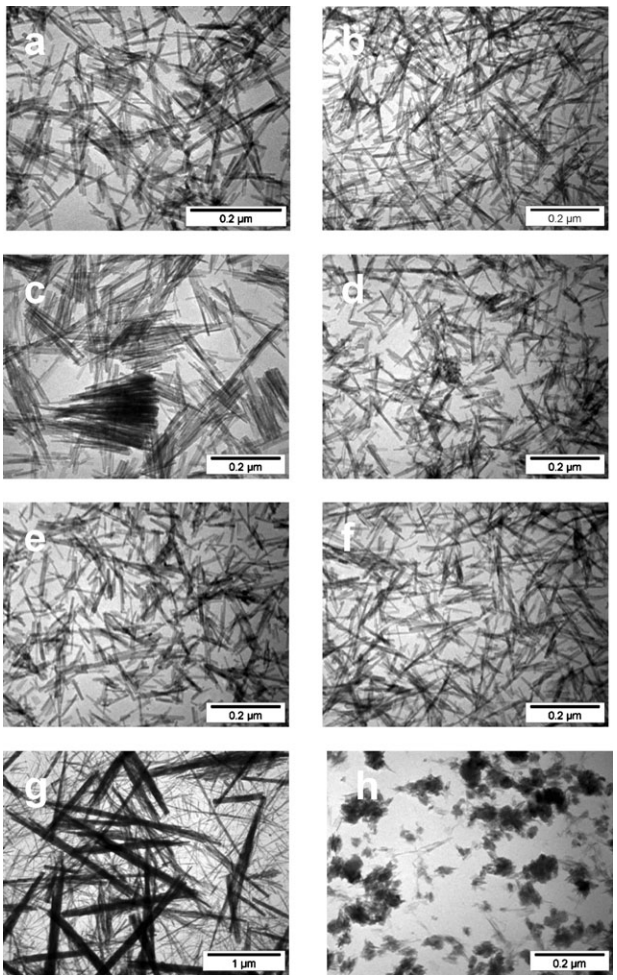

Fig. 2 LRTEM micrographs of as-synthesized $LnPO_4 \cdot nH_2O$ nanostructures obtained after microwave heating: (a) La, (b) Ce, (c) Nd (d) Sm, (e) Eu, (f) Gd, (g) Tb and (h) Er.

Transmission electron microscopy

Fig. 2 represents the LRTEM micrographs of the as-synthesized hydrated hexagonal $LnPO_4 \cdot nH_2O$ (Ln = La, Ce, Nd, Sm, Eu, Gd and Tb) nanorods/nanowires, and the bct $ErPO_4 \cdot nH_2O$ nanoparticles. $NdPO_4 \cdot nH_2O$ [Fig. 2(c)] and $TbPO_4 \cdot nH_2O$ [Fig. 2(g)] resemble a bundle of nanorods and nanowires, respectively. The as-synthesized $LnPO_4 \cdot nH_2O$ products (Ln = La, Ce, Nd, Sm, Eu and Gd) consist, in most cases, of nanorods with a diameter of 6–9 nm and lengths ranging from 70 to 800 nm. The $TbPO_4 \cdot nH_2O$ nanowires [Fig. 2(g)] are 0.5 to 1.5 μm in length and 6 to 8 nm in width and the $TbPO_4 \cdot nH_2O$ nanorods are 1.1 to 2.2 μm in length and 80 to 130 nm in width. Because of the lanthanide contraction, a different phase is formed for erbium phosphate, which leads to a different morphology, that is, particles (20 to 100 nm). The particle shape for the Er sample may be a consequence of not having a preferred growth direction as compared to all the other hexagonal samples. In addition, the TEM micrographs of the $ErPO_4$ phase reveal a mixture of aggregates and nanoparticles, meaning that the sample is not homogeneous.

Fig. 3 (see also Fig. S1 in electronic supporting information, ESI) shows the HRTEM micrographs of (i) a mixture of nanorods/nanowires (A1–C1, see also D1–F1 in the ESI), (ii) a single nanorod/nanowire (A2–C2, see also D2–F2 in the ESI), and (iii) corresponding selected area electron diffraction (SAED) patterns (A3–C3, see also D3–F3 in the ESI) of $LnPO_4 \cdot nH_2O$ nanostructures. Fig. 3(A1, Bl Cl) [and Fig. S1(Dl, El Fl) in the ESI] clearly show $LnPO_4 \cdot nH_2O$ nanorods, except for $TbPO_4 \cdot nH_2O$, which shows a mixture of nanowires and

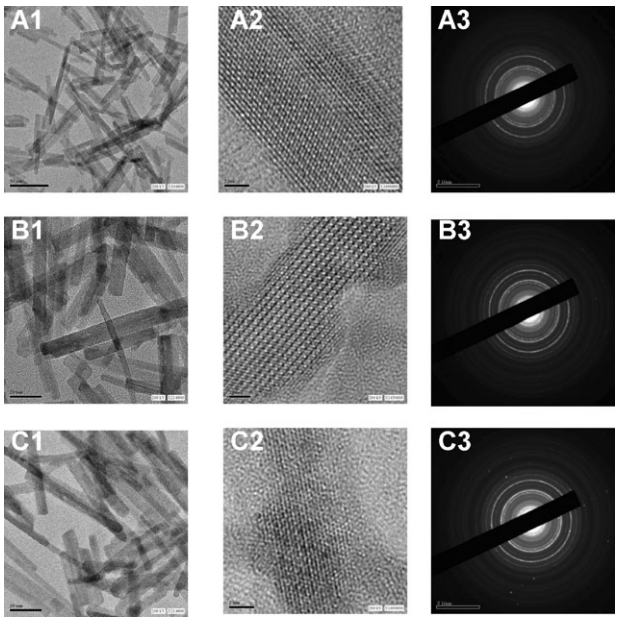

Fig. 3 HRTEM micrographs of as-synthesized $LnPO_4 \cdot nH_2O$ nanorods [Ln = La (A1–3), Eu (Bl–3), and Gd (Cl–3)]: (i) nanorods (AI, Bl & Cl); (ii) micrograph of a single nanorod (A2–C2) with clear lattice fringes; and (iii) corresponding SAED pattern (A3–C3).

nanorods [Fig. S1(Fl) in the ESI]. The clear lattice fringes in the HRTEM micrographs [Fig. 3(A2, B2, C2), see also Fig. S1(D2, E2, F2) in the ESI] confirm the high crystallinity of the nanorods. For example, in the case of $LaPO_4 \cdot nH_2O$ [Fig. 3(A2)], the spacings between two adjacent horizontal and two adjacent vertical lattice planes of 3.15 and 2.86 Å, respectively, compare well with the corresponding theoretical interplanar spacings of 3.072 49 and 2.868 Å, respectively, for hexagonal phase $LaPO_4 \cdot nH_2O$ (JCPDS No. 46-1439).‡ Combined with the results of fast Fourier transform (FFT) analysis (not shown here), they are found to correspond to the (200) and (102) planes, respectively, of $LaPO_4 \cdot nH_2O$. The corresponding SAED pattern of $LaPO_4 \cdot nH_2O$ rods is shown in [Fig. 3(A3)]. The continuous rings may be the indication of the electron diffraction of a bunch of nanorods. The electron diffraction spots are calculated to have, approximately, d spacings of 6.12, 4.46, 3.1, 2.86 and 2.16 Å, which correspond to the 100, 101, 200, 102 and 003 crystal planes, respectively, and can be indexed to a pure hexagonal phase. This result corroborates the XRD analysis. Similarly, the other $LnPO_4 \cdot nH_2O$ (Ln = Ce, Sm, Eu, Gd and Tb) nanorods can also be indexed to the hexagonal phases based on the XRD and SAED results. The energy dispersive X-ray spectroscopy (EDS) analysis of an individual nanorod or nanowire indicates that the particle is composed mainly of the Ln, P, and O elements. EDS analysis gives an Ln : P : O atomic ratio of ~1 : 1 : 4 to 1 : 1 : 4.5, in agreement with the proposed stoichiometry $LnPO_4 \cdot nH_2O$ and indicating that the $LnPO_4$ contain crystallization water with n = 0.3 to 1.0 (Table 1).

Thermogravimetry (TG) and differential scanning calorimetry (DSC) analyses

Representative $LnPO_4 \cdot nH_2O$ (Ln = La, Ce, Sm) TGA-DSC profiles are shown in Fig. 4. In the case of $LaPO_4 \cdot 0.5H_2O$ [Fig. 4(a)], two weight losses occur in two distinct steps with an overall weight loss of 7.4% between 20 to 500 °C. The first weight loss corresponds to a broad endothermic peak in the

‡ For Eu [Fig. 3(B2)], d_{102} = 0.279 nm and d_{003} = 0.216 nm; for Gd [Fig. 3(C2)], d_{200} = 0.298 nm (major) and d_{102} = 0.281 nm

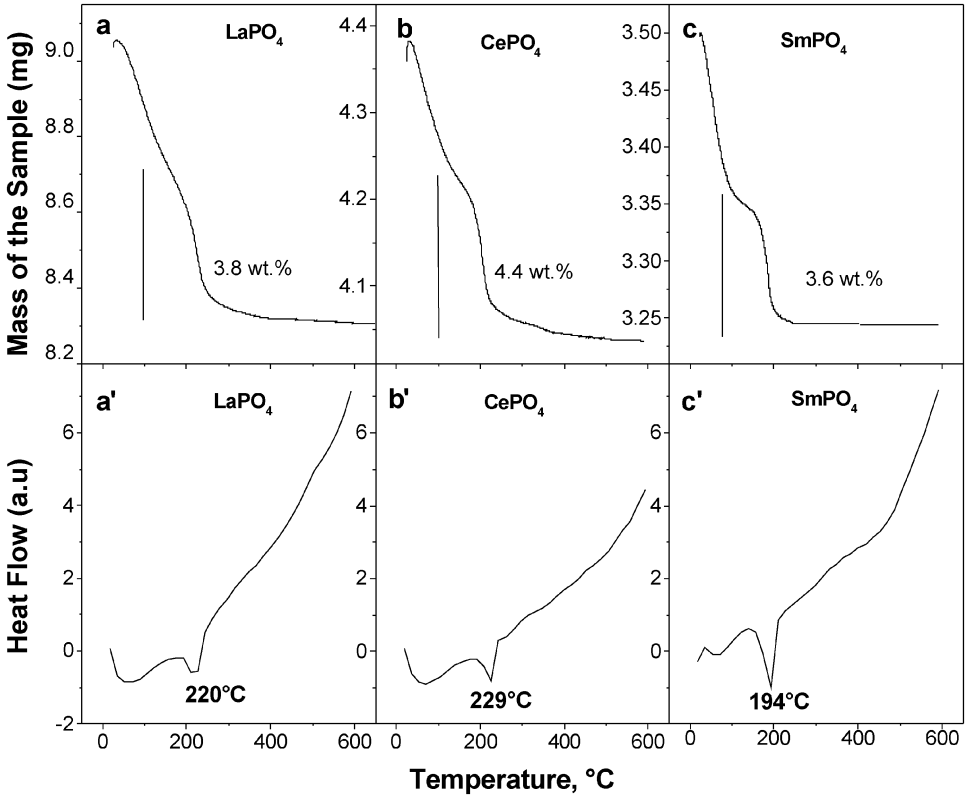

Fig. 4 Thermogravimetric analysis (a–c) and differential scanning calorimetry analysis (a′–c′) of the as-synthesized $LnPO_4 \cdot nH_2O$ (Ln = La, Ce and Sm).

temperature range 20–100 °C in the DSC curve [Fig. 4(a′)]. It is assigned to the release of 3.6 wt % of residual water, which is physically adsorbed on the surface of the as-synthesized material. The second weight loss (3.8 wt %) corresponds to loss of the 0.5 moles of H_2O as the hexagonal $LaPO_4 0.5H_2O$ dehydrates; this begins around 180 °C to finish at 500 °C. A corresponding well-defined endothermic peak is observed by DSC in the temperature range 180–250 °C with a sharp peak at 220 °C. This second weight loss can be schematically represented as follows:[22]

$$LaPO_4 \cdot 0.5H_2O\ _{(hexagonal)} + \Delta \rightarrow LaPO_4\ _{(hexagonal)} + 0.5\ H_2O\uparrow$$

A similar behavior is observed with $CePO_4 \cdot H_2O$ [Fig. (4b,b′)] and $SmPO_4 \cdot 0.5H_2O$ [Fig. 4(c,c′)].

FTIR and Raman spectroscopy

Most of the FTIR bands of the as-synthesized $LnPO_4 \cdot nH_2O$ (Ln = La, Ce, Nd, Sm, Eu, Gd, Tb and Er) materials are characteristic of the vibrations of the phosphate (PO_4^{3-}) groups (see Fig. S2 in the ESI).[23] Three bands, located at 542, 570 and 615 cm^{-1}, are clearly observed in the v_4 region of the vibrations of the PO_4^{3-} groups. Although we expect two separate vibrational bands at 1015 and 1050 cm^{-1} for the v_3 vibrations of the PO_4^{3-} groups, they are not clearly resolved in the FTIR spectra because of the low resolution. The v_2 vibration is not observed in the investigated range of wave numbers. The shoulder at 960 cm^{-1} is assigned to the v_1 vibration of the PO_4^{3-} groups. The present FTIR data for lanthanide orthophosphates match other reported values[2,24–27] and show the presence of a discrete PO_4^{3-} group; no pyrophosphate (P_2O_7 group, a typical band appearing at 1265–1267 cm^{-1}) impurity is detected.[23]

The Raman spectra of rhabdophane-type $LnPO_4 \cdot nH_2O$ have been previously characterized (see also Fig. S3 in the ESI).[21,22,25] The most intense Raman band for all the rhabdophane-type $LnPO_4 \cdot nH_2O$ is observed at 988 ± 10 cm^{-1} and is assigned to the *A* mode, with totally symmetric vibration. Seven or eight phosphate bending modes are predicted in point groups D_6 or D_3 for each Raman spectrum between 642–400 cm^{-1}.[26] The bending modes over 500 cm^{-1} are the asymmetric vibrational modes. However, because of the low resolution, not all the peaks could be clearly observed.

XPS spectroscopy

The XPS spectra of hexagonal $LnPO_4 \cdot nH_2O$ (Ln = La, Ce and Nd) nanorods are shown in Fig. 5 and Figs S4 and S5 in the ESI. The binding energy data [calibrated using C 1s (284.8 eV) as the reference] from the $LaPO_4 \cdot nH_2O$,[2,26] $CePO_4 \cdot nH_2O$[26] and $NdPO_4 \cdot nH_2O$[27] XPS spectra are consistent with those reported for bulk $LnPO_4$ (Ln = La, Ce and Nd).[2,27] The peak at 835.23 eV for $LaPO_4 \cdot nH_2O$ [Fig. 5(b)], 885.03 eV for $CePO_4 \cdot nH_2O$ [Fig. S4(b) in the ESI], and 982.73 eV for $NdPO_4 \cdot nH_2O$ [Fig. S5(b) in the ESI] indicate the binding energies of the $3d_{5/2}$ orbital of La^{3+}, Ce^{3+}, and Nd^{3+}, respectively, in the corresponding $LnPO_4 \cdot nH_2O$ products. The La 3d line [Fig. 5(b)] and the Ce 3d line [Fig. S4(b) in the ESI] are characterized by a better resolution between the main lines and the corresponding satellites, which corroborates earlier literature.[26] The peak at 133.5 eV [P 2p, Fig. 5(c), Fig. S4 and S5 in the ESI] for all the $LnPO_4 \cdot nH_2O$ (Ln = La, Ce and Nd) indicates that the phosphorus in the products exists in a pentavalent oxidation state (P^{5+}) in the form of PO_4.[2,28] The peak at 531.2 eV [O 1s, Fig. 5(d), Figs. S4 and S5 in the ESI] for all the $LnPO_4 \cdot nH_2O$ corresponds to the literature data.

Photoluminescence properties

The excitation and emission spectra of $EuPO_4 \cdot nH_2O$ nanorods are shown in Fig. 6(a) and Fig. 6(a′), respectively. The excitation spectrum of Eu^{3+} exhibits an intense band at 393 nm caused by the direct excitation of the Eu^{3+} ground state into higher levels of the 4f manifold (such as $^7F_0$–$^5L_6$ at

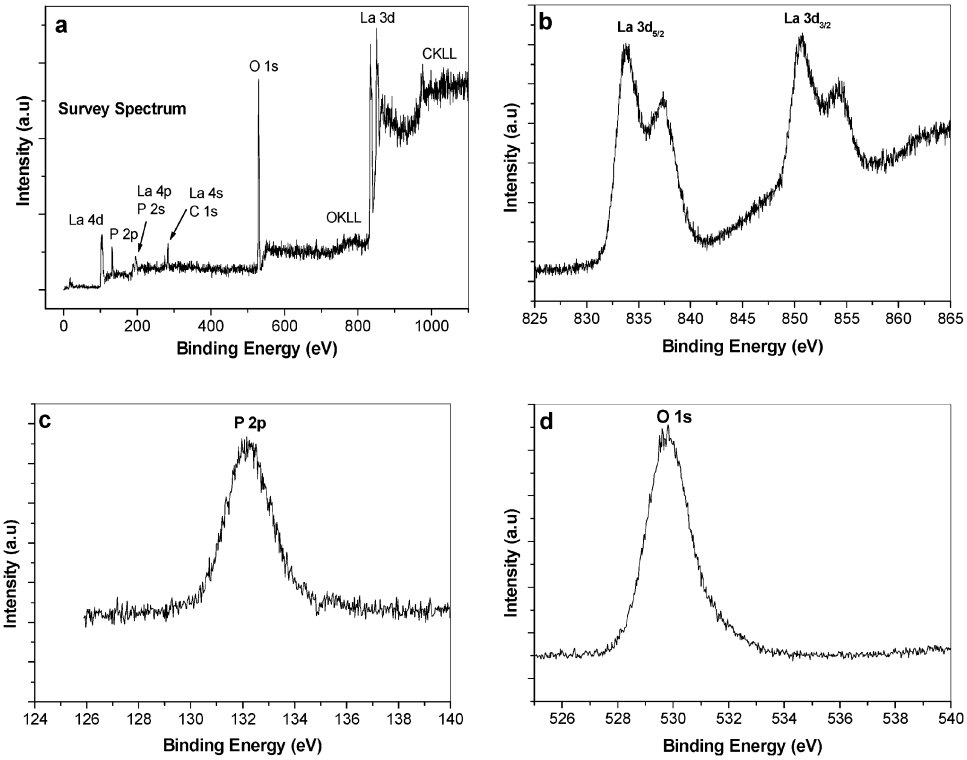

Fig. 5 X-Ray photoelectron spectra (XPS) of as-synthesized hexagonal $LaPO_4 \cdot nH_2O$ nanorods/nanowires by microwave heating: (a) survey spectrum, (b) La 3d region, (c) P $2p_{3/2}$, (d) O 1s.

393 nm).[29–31] Upon excitation of Eu^{3+} at 393 nm, the emission spectrum of $EuPO_4 \cdot nH_2O$ nanorods consists of sharp lines, as expected for the transitions between europium levels. The emission spectrum is composed of a $^5D_0$–^7F_J (J = 1, 2, 3, 4) manifold of emission lines of Eu^{3+}, with the magnetic-dipole-allowed $^5D_0$–$^7F_1$ transition (588 nm) being the most prominent emission line. This transition is stronger than the electric dipole $^5D_0$–$^7F_2$ transition of Eu^{3+} due to the effects of phosphate groups in $EuPO_4 \cdot nH_2O$. The $^5D_0$–$^7F_2$ transition splits into three components, while the $^5D_0$–$^7F_1$ transition (magnetic dipole in character) splits into two components in $EuPO_4 \cdot nH_2O$ (although it is not nicely resolved here). The presence of

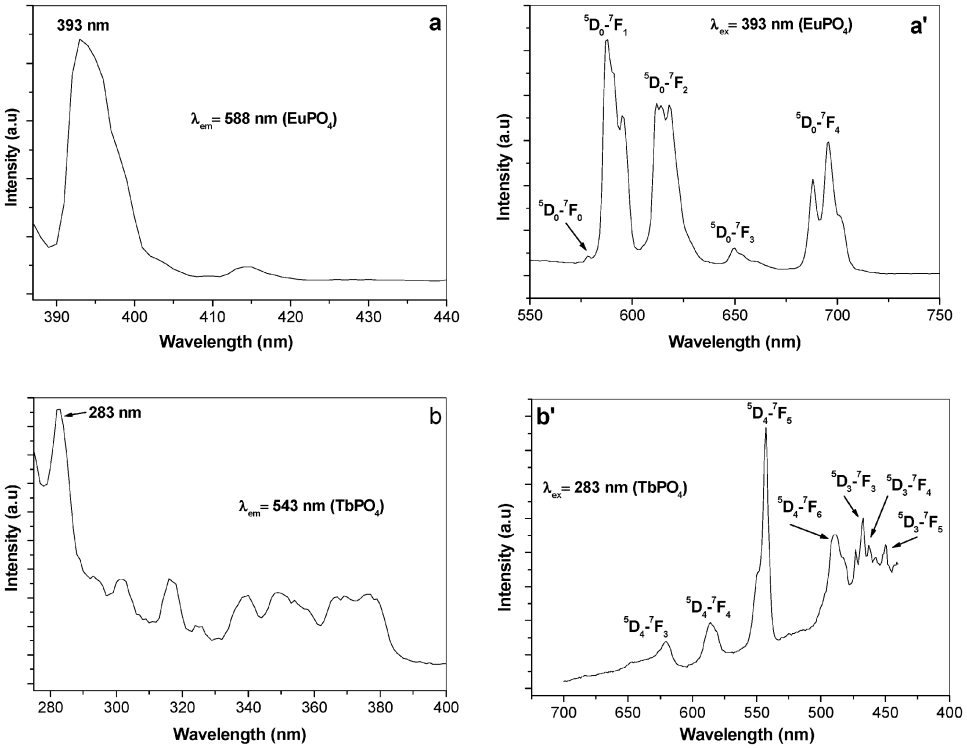

Fig. 6 Excitation and emission spectra of as-synthesized hexagonal $EuPO_4 \cdot nH_2O$ (a and a′, respectively) and $TbPO_4 \cdot nH_2O$ (b and b′, respectively) nanorods/nanowires.

a sensitive, forbidden $^5D_0$–$^7F_0$ transition has been identified with a very weak intensity. Figs. 6 (b,b′) show the excitation and emission spectra of $TbPO_4 \cdot nH_2O$ nanorods. Exciting $TbPO_4 \cdot nH_2O$ at 283 nm (due to the f–f transitions within the Tb^{3+} $4f^8$ electronic configuration) yields the characteristic blue $^5D_4$–$^7F_{J'}$ (J' = 4,5) and green $^5D_3$–^7F_J (J = 3, 4, 5, 6) emission of Tb^{3+}, with the $^5D_4$–$^7F_5$ (543 nm) green emission being the most prominent band [Fig. 6(b′)].[29,32]

Proposed mechanism

The exact mechanism for the formation of $LnPO_4 \cdot nH_2O$ (Ln = La–Tb) nanorods/nanowires using microwave irradiation under solvothermal condition needs to be further investigated. The following proposed mechanism is based on reported conventional heating methods.[2,4,5,33,34] Fang *et al.*[2] reported that the formation of single crystal lanthanide orthophosphate nanorods/nanowires under hydrothermal conditions (12 h at 150 °C) follows the spherical, diffusion-controlled crystal growth theory (in surfactant-free systems).[33] This theory could also explain the formation of $LnPO_4 \cdot nH_2O$ nanorods/nanowires using microwave irradiation.

On the other hand, the $LnPO_4 \cdot nH_2O$ (Ln = La–Tb) nanorods/nanowires that have been fabricated here have a hexagonal crystal structure, similar to that of ZnO[35] and $Ln(OH)_3$,[16,34] which are known to exhibit anisotropic growth. In principle, the anisotropic growth of a crystal should be favorable for the formation of nanorods. Because of the hexagonal crystal structures observed here, which are characteristic of highly anisotropic growth, we believe that the habit of anisotropic growth is the inherent reason for the formation of $LnPO_4 \cdot nH_2O$ nanorods/nanowires.

In these reactions temperature is the dominant factor affecting the reactivity. The interaction between the high-frequency electromagnetic radiation (2.45×10^9 Hz) and the permanent dipole moment of the precursors results in molecular rotations, which lead to the rapid volumetric heating of the liquid phase.[36–39] We have also carried out a series of experiments with $SmPO_4 \cdot nH_2O$ under similar reaction conditions at different irradiation times (1, 10 and 20 min). In all cases, nanorods are exclusively obtained (data not presented here). Particles, which, in many cases, are the first step in the formation of nanowires/nanorods, were not observed.[40–42] Compared to conventional heating methods,[2,4,5] microwave dielectric heating presents a much more rapid and simultaneous nucleation due to the fast and homogeneous heating effects of microwaves. We suggest that the high microwave susceptibility of water (dielectric constant ε = 80.4)[36,37,40] makes it an excellent microwave-absorbing agent, thus leading to high heating rates and significantly shortened reaction times. The movement and polarization of water molecules under the rapidly changing electric field of the microwave reactor may result in transient, anisotropic microdomains for the reaction system, facilitating the anisotropic growth of $LnPO_4 \cdot nH_2O$ nanorods/nanowires.

The exact mechanism and the effect of the concentration of $NH_4H_2PO_4$ (affecting pH) on the morphology of $LnPO_4 \cdot nH_2O$ nanorods/nanowires are still under investigation.

Conclusions

Rhabdophane-type hexagonal $LnPO_4 \cdot nH_2O$ (Ln = La, Ce, Nd, Sm, Eu, Gd, Tb) nanorods/nanowires and body-centered tetragonal $ErPO_4 \cdot nH_2O$ nanoparticles (formation of different phases of $LnPO_4 \cdot nH_2O$ depends on the ionic radius of the lanthanide ions) have been successfully synthesized on a large scale by refluxing a mixture of an aqueous solution of Ln(III) nitrate and an $NH_4H_2PO_4$ solution under solvothermal conditions by microwave heating in a simple domestic microwave oven. The structure, morphology, chemical composition and physical properties of the as-prepared products have been characterized thoroughly by different analytical tools. The microwave-assisted products are obtained pure, in high yields, and are structurally uniform and well-crystallized. The method does not need high temperatures (though local high temperatures are obtained), high pressures, catalyst, templates, surfactants, vacuum conditions or preprocessing. It is simple, fast, clean, efficient, economically cheap, nontoxic, and eco-friendly. All these are important considerations for industrial manufacturing. Furthermore, we believe that this microwave method could be extended to the fabrication of many other nanoscale materials, such as $AlPO_4$, $GaPO_4$, $InPO_4$ and $ZnPO_4$.

Acknowledgements

Dr C. R. Patra and Prof. A. Gedanken thank the EC for a research grant IST-2001-39112 awarded through the 5th Program of the NANOPHOS Consortium.

References

1 R. M. Penner, *Acc. Chem. Res.*, 2000, **33**, 78.
2 Y.-P. Fang, A.-W. Xu, R.-Q. Song, H.-X. Zhang, L.-P. You, J.-C. Yu and H.-Q. Liu, *J. Am. Chem. Soc.*, 2003, **125**, 16025.
3 Y. N. Xia, P. D. Yang, Y. G. Sun, Y. Y. Wu, B. Mayers, B. Gates, Y. D. Yin, F. Kim and H. Q. Yan, *Adv. Mater.*, 2003, **15**, 353, and references therein.
4 Y.-W. Zhang, Z.-G. Yan, L.-P. You, R. Si and C.-H. Yan, *Eur. J. Inorg. Chem.*, 2003, 4099.
5 Z.-G. Yan, Y.-W. Zhang, L.-P. You, R. Si and C.-H. Yan, *J. Crystal Growth*, 2004, **262**, 408.
6 Y. W. Zhang, Y. Yang, S. Jin, S. J. Tian, G. B. Li, J. T. Jia, C. S. Liao and C. H. Yan, *Chem. Mater.*, 2001, **13**, 372.
7 Z. J. Wei, L. D. Sun, C. S. Liao, J. L. Yin, X. C. Jiang, C. H. Yan and S. Z. Lu, *J. Phys. Chem. B*, 2003, **106**, 10610.
8 Y. Hikichi and T. Nomura, *J. Am. Ceram. Soc.*, 1987, **70**, C-252.
9 F. H. Firsching and S. N. Brune, *J. Chem. Eng. Data*, 1991, **36**, 93.
10 Y. Guo, P. Woznicki, A. Barkatt, E. E. Saad and I. G. Talmy, *J. Mater. Res.*, 1996, **11**, 639.
11 K. Riwotzki, H. Meyssamy, H. Schnablegger, A. Komowski and M. Haase, *Angew. Chem., Int. Ed.*, 2001, **40**, 573.
12 K. Riwotzki, H. Meyssamy, A. Komowski and M. Haase, *J. Phys. Chem. B*, 2000, **104**, 2824.
13 G. Carini, G. D. Angelo, G. Tripodo, A. Fontana, F. Rossi and G. A. Saunders, *Europhys. Lett.*, 1997, **40**, 435.
14 G. Sarala Devi, D. Giridhar and B. M. Reddy, *J. Mol. Catal. A: Chem.*, 2002, **181**, 173.
15 H. Meyssamy and K. Riwotzki, *Adv. Mater.*, 1999, **11**, 840.
16 A. W. Xu, Y. P. Fang, L. P. You and H. Q. Lin, *J. Am. Chem. Soc.*, 2003, **125**, 1494.
17 W.-G. Xu, Y.-G. Tian, M. Liu, H. T. Liu, G.-H. Fang and W.-Q. Pang, *Gaodeng Xuexiao Huaxue Xuebao*, 1996, **17**, 1513.
18 H. Assaaoudi, A. Ennaciri and A. Rulmont, *Vib. Spectrosc.*, 2001, **25**, 81.
19 Y. Hikichi, K. Hukuo and J. Shiokawa, *Bull. Chem. Soc. Jpn.*, 1978, **51**, 3645.
20 O. Palchik, I. FeIner, G. Katabyand and A. Gedanken, *J. Mater. Res.*, 2000, **15**, 2176.
21 S. Lucas, E. Champion, D. Bregiroux, D. Bernache-AssoIlant and F. Audebert, *J. Solid State Chem.*, 2004, **177**, 1302.
22 S. Lucas, E. Champion, D. Bernache-AssoIlant and G. Leroy, *J. Solid State Chem.*, 2004, **177**, 1312.
23 A. Hezel and S. D. Ross, *Spectrochim. Acta*, 1966, **22**, 1949.
24 R. Kijkowska, E. Cholewka and B. Duszak, *J. Mater. Sci.*, 2003, **38**, 223.
25 G. M. Begun, G. W. Beall, L. A. Boatner and W. J. Gregor, *J. Raman Spectrosc.*, 1981, **11**, 273.
26 O. P. Ivanova, L. A. Vasilyev, A. V. Naumkin and V. V. Kantsel, *Appl. Surf. Sci.*, 1993, **72**, 307.
27 H. Guan and Y. Zhang, *J. Solid State Chem.*, 2004, **177**, 781.
28 J. C. Yu, L. Z. Zhang, Z. Zheng and J. C. Zhao, *Chem. Mater.*, 2003, **15**, 2280.
29 U. Rambabu, N. R. Munirathnam, T. L. Prakash and S. Buddhudu, *Mater. Chem. Phys.*, 2002, **78**, 160.
30 N. El Jouhari, C. Parent and G. Le Flem, *J. Solid State Chem.*, 1996, **123**, 398.
31 Y.-J. Wang, W. Zhao and M.-Z. Su, *J. Lumin.*, 1988, **40–41**, 177.

32 G. Blasse and B. C. Grabmaier, *Luminescent Materials*, Springer-Verlag, Berlin, Heidelberg, 1994.
33 Z. A. Peng and X. G. Peng, *J. Am. Chem. Soc.*, 2002, **124**, 3343.
34 X. Ma, H. Zhang, Y. Ji, J. Xu and D. Yang, *Mater. Lett.*, 2004, **58**, 1180.
35 M. Huang, S. Mao, H. Feick, H. Yan, Y. Wu, H. Kind, E. Weber, R. Russo and P. Yang, *Science*, 2001, **292**, 1897.
36 S. A. Galema, *Chem. Soc. Rev.*, 1997, **26**, 233, and references therein.
37 C. R. Patra and A. Gedanken, *New J. Chem.*, 2004, **28**, 1060.
38 P. Lidstrom, J. Tierney, B. Wathey and J. Westman, *Tetrahedron*, 2001, **57**, 9225.
39 D. Michael, P. Mingos and D. R. Baghurst, *Chem. Soc. Rev.*, 1991, **20**, 1.
40 S. J. Doktycz and K. S. Suslick, *Science*, 1990, **247**, 1067.
41 J. M Zhu, K. Yang, J. J. Zhu, G. B. Ma, X. H. Zhu, S. H. Zhou and Z. G. Liu, *Opt. Mater.*, 2003, **23**, 89.
42 C. R. Patra, Y. Mastai and A. Gedanken, *J. Nanoparticle Res.*, 2004, **6**, 509.